







High-Speed and High-Resolution Microwave Photonic Interrogation of a Fiber-Optic Refractometer With Plasmonic Spectral Comb

Guangying Wang , Yuan Cao , Nan Hu, Xuejun Zhang, Shaochen Duan, Tuan Guo , *Member, IEEE, Member, OSA*, Xinhuan Feng , Bai-Ou Guan , *Member, IEEE, Fellow, OSA*, and Jianping Yao , *Fellow, IEEE, Fellow, OSA*

Abstract—Microwave photonic interrogation of a high-speed and high-resolution refractive index (RI) sensor based on a tilted fiber Bragg grating with surface plasmon resonance (TFBG-SPR) is proposed and experimentally demonstrated. Instead of demodulating the wavelength shift or intensity change of a TFBG-SPR spectrum in the optical domain, we convert the TFBG-SPR spectrum to the time domain based on spectral shaping (SS) and wavelength-to-time (WTT) mapping and use a digital signal processor (DSP) to extract the RI information at a high speed and high resolution. In the experiment, when an Au-coated TFBG is immersed in a solution, the TFBG-SPR spectrum will produce a dip. When the RI changes, the location of the dip in the TFBG-SPR spectrum will shift, which is a function of the RI. By passing a broadband frequency-chirped optical pulse generated by a frequency swept laser source to the TFBG-SPR and detecting the optical pulse at the output of the TFBG-SPR at a photodetector (PD), due to SS-WTT mapping, a temporal waveform with its shape identical to the optical spectrum is produced. A DSP is then used to extract the SPR envelope information from the temporal waveform. By monitoring the changes of the SPR envelope, the RI information is interrogated with a high resolution of 1.123×10^{-6} RIU at a high speed over 20 kHz.

Index Terms—Microwave photonics, refractive index measurement, surface plasmon resonance, tilted fiber Bragg grating.

Manuscript received September 21, 2019; revised December 10, 2019; accepted December 11, 2019. Date of publication December 13, 2019; date of current version April 1, 2020. This work was supported in part by National Natural Science Foundation of China (NSFC) under Grant 61860206002, Grant 61701193, Grant 61771221, and Grant 61975068 and in part by the Special Funds for the Cultivation of Guangdong College Students' Scientific and Technological Innovation (pdjh2018a0053). (*Corresponding authors: Yuan Cao; Xinhuan Feng.*)

G. Wang, Y. Cao, N. Hu, X. Zhang, S. Duan, T. Guo, X. Feng, and B.-O. Guan are with the Guangdong Province Key Laboratory of Optical Fiber Sensing and Communications, Institute of Photonics Technology, Jinan University, Guangzhou 510632, China (e-mail: guangyingwang@stu2017.jnu.edu.cn; caoyuan@jnu.edu.cn; huhu123@stu2017.jnu.edu.cn; zxjun24@gmail.com; duanshaochen@stu2016.jnu.edu.cn; tuanguo@jnu.edu.cn; eexhfeng@gmail.com; tguanbo@jnu.edu.cn).

J. Yao is with the Microwave Photonics Research Laboratory, School of Electrical Engineering and Computer Science, University of Ottawa, Ottawa, ON K1N 6N5, Canada (e-mail: jpyao@eecs.uottawa.ca).

Color versions of one or more of the figures in this article are available online at <http://ieeexplore.ieee.org>.

Digital Object Identifier 10.1109/JLT.2019.2959665

I. INTRODUCTION

A TILTED fiber Bragg grating (TFBG) is a special fiber grating that has a comb like spectrum which shares all the advantages of a regular fiber Bragg grating including compact size, low cost, immunity to electromagnetic interference and high tolerance to harsh environment. TFBGs have been widely employed for applications such as mechanical sensing [1], [2], biomedical sensing and chirped microwave waveform generation [3]. For most of the biomedical sensing applications, the refractive index (RI) of a solution is a key parameter to characterize a bio-sample under test [4]–[6]. Usually, the RI change in a bio-sample is very small and a sensor based on a regular TFBG will not provide sufficiently high sensitivity to monitor the change. To improve the RI sensitivity, introducing a surface plasmon resonance (SPR) to a regular TFBG has been studied [7]–[10]. Recently, numerous biomedical and electrochemical sensing applications, such as the detection of urinary protein variations [11], the detection of density alteration in cells [12], the measurement of glucose concentrations [13], and the detection of the state of charge of supercapacitors for renewable energy storage [14] based on a TFBG-SPR have been proposed and experimentally demonstrated. To excite the SPR effect in a regular TFBG, a nanoscale Au-coating is planted on the surface of the regular TFBG. When an Au-coated TFBG is immersed in a solution under test, a dip will be produced in the spectrum. As the ambient RI changes, the location of the dip in the TFBG-SPR spectrum will be a function of the RI. By monitoring the change of the TFBG-SPR spectrum, the sensing information can be demodulated. For most TFBG-SPR sensing demodulation methods, an optical spectrum analyzer (OSA) is used to monitor the change of the TFBG-SPR spectrum. However, it is very complicated to monitor the spectrum change of a TFBG-SPR in the optical domain, since the cladding mode where the SPR is located has to be tracked first, and then the intensity change of the adjacent cladding mode is marked to demodulate the RI change. If the SPR switches to a new cladding mode, the new cladding mode should be identified and tracked, which means a continuous demodulation in a large range of the RI change cannot be achieved by simply marking a specific cladding mode. Moreover, an OSA usually has a very low wavelength resolution and slow scanning speed. When a

rapid and small RI change caused by biomedical reactions such as molecular adhesion [15], [16] is to be measured, the use of an OSA will not have the ability to detect the change. Till now, no effective demodulation methods have been demonstrated for a sensor employing a TFBG-SPR.

Microwave photonics (MWP) [17] is a technique to process microwave signals directly in the optical domain at a high speed and high resolution. In addition to the applications in optical communications [18] and radar systems [19], microwave photonics has a high potential for applications in high speed and high accuracy sensing [20], [21]. To avoid using the wavelength marking technique or the intensity measuring technique which is complicated and has low accuracy and poor resolution, the sensing information can be demodulated in the time domain.

In this paper, we report the use of a microwave photonic technique based on spectral shaping and wavelength-to-time (SS-WTT) mapping [22], [23] to convert the spectrum of a TFBG-SPR to the time domain, to increase the speed and resolution of a TFBG-SPR sensor. In a SS-WTT mapping system, the spectrum of a broadband light source is shaped by an optical filter (spectral shaping or SS) and the shaped spectrum is converted to the time domain in a dispersive element to achieve wavelength-to-time (WTT) mapping. If the dispersive element has linear dispersion, the WTT mapped time-domain signal will have the same shape as the shaped spectrum. The SS-WTT mapping technique has been reported for applications such as high-speed analog-to-digital conversion [24] and microwave waveform generation [22], [23]. However, no reports have been published for TFBG-SPR sensing. In the proposed sensing system, a high-speed frequency swept laser source is used to generate a high-speed and broadband frequency-chirped optical pulse which is applied to an Au-coated TFBG. Through SS-WTT mapping, the sensing information encoded in the optical domain is converted to the time domain. By detecting the optical pulse from the Au-coated TFBG at a photodetector (PD), a temporal waveform with its shape identical to the shaped optical spectrum is generated. Specifically, when the ambient RI is changed, a dip in the envelope of the temporal waveform detected at the output of the PD will shift due to the TFBG-SPR spectrum change. By using a digital signal processor (DSP), the sensing information can be extracted at a high speed and high resolution. More importantly, by using the SS-WTT mapping technique, the sensing information can be continuously demodulated. The proposed RI sensor is experimentally demonstrated. The RI sensing resolution and sensitivity are 1.123×10^{-6} refractive index unit (RIU) and $142.496 \mu\text{s}/\text{RIU}$, respectively, and the sensing speed is as high as 23.496 kHz.

II. PRINCIPLE

The optical spectrum of a regular TFBG has a series of cladding modes with a relatively flat spectrum distribution. By plating a nanoscale Au-coating on the surface of a TFBG, SPR effect will be excited and the power distribution of the cladding mode peaks will be changed to introduce a dip when the Au-coated TFBG is immersed in a solution under

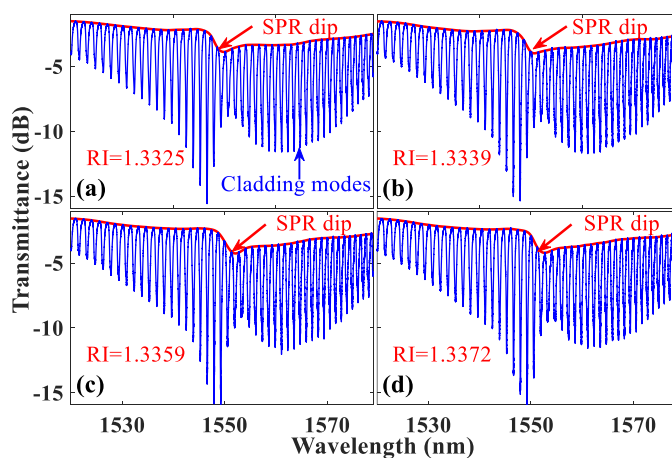


Fig. 1. Transmission spectrum of a TFBG-SPR. An SPR dip is observed and its location is changed when the ambient RI is changed from (a) 1.3325, (b) 1.3339, (c) 1.3359, to (d) 1.3372.

test. Fig. 1(a) shows the transmission spectrum of an Au-coated TFBG when the ambient RI is 1.3325. As can be seen, the transmission spectrum of the TFBG has multiple peaks induced due to the cladding modes (shown as the blue curve). The power distribution of these cladding mode peaks is modulated by a dip (as the red curve shown) which is introduced due to the SPR effect. The transmission spectrum of the cladding modes, after WTT mapping, corresponds to a temporal signal with its envelope modulated by the SPR dip. As can be seen, at the wavelength of about 1550 nm, the power distribution of the cladding modes is distorted and a dip is introduced due to the SPR effect. When the ambient RI is changed, the location of the dip will shift.

Normally, to demodulate the RI information in the optical domain, the cladding mode where the SPR is located is marked and the intensity change of the adjacent cladding mode is measured as the ambient RI is increasing. Once the RI change exceeds a threshold, the SPR will shift to another cladding mode, marking the previous cladding mode and measuring the intensity change of the adjacent cladding mode will no longer be applicable. Fig. 1(b), (c) and (d) show the experimentally measured SPR shifts versus RI change. We can see that the SPR is shifted from 1552 nm to 1553.5 nm and from 1553.5 nm to 1554.75 nm when the ambient RI is increased from 1.3339 to 1.3359 and from 1.3359 to 1.3372, respectively. In addition, due to the mechanical nature of the wavelength scanning mechanism inside an OSA, the sensing speed is very low, which will further deteriorate the sensing performance when a rapidly changing bio-sample is under test. In fact, we can consider that when the ambient RI is changing, the spectrum of the SPR will lead to a continuously changing envelope in the optical domain. However, this envelope change cannot be demodulated continuously in the optical domain due to the limited number of cladding modes of a TFBG. Therefore, if we can extract the envelope, the sensing information can be continuously demodulated by monitoring the change of the extracted envelope.

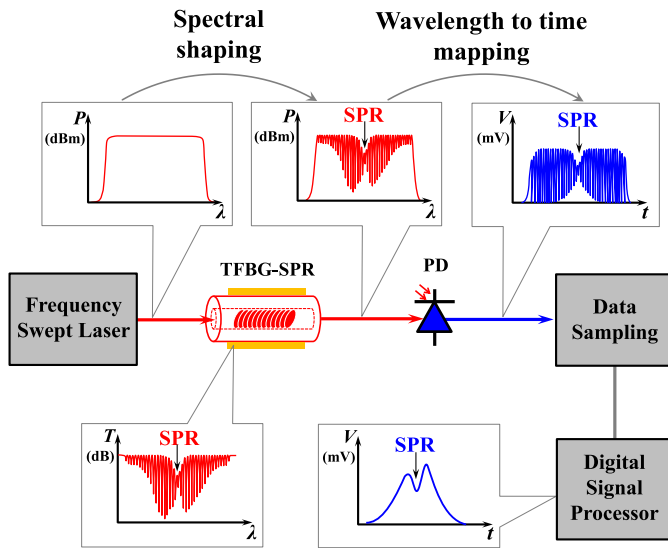


Fig. 2. Schematic diagram of the proposed sensing system.

Based on the analysis of the demodulation method for the TFBG-SPR mentioned above, to avoid using the wavelength marking or the intensity monitoring method which is complicated and has low accuracy and resolution, and to extract the SPR envelope, we propose to use a microwave photonic technique to convert the spectrum of a TFBG-SPR to the time domain based on SS-WTT mapping, and detect the TFBG-SPR envelope using a DSP.

The proposed sensing system is shown in Fig. 2. It consists of a frequency swept laser source, a TFBG-SPR, a PD, an oscilloscope, and a DSP. The frequency swept laser source is used to generate a broadband frequency-chirped optical pulse. Due to the frequency chirp nature of the pulse, a specific relationship between the instantaneous wavelength and time is established. By passing a broadband frequency-chirped optical pulse generated by the frequency swept laser source to the TFBG-SPR, the sensing information is encoded in the optical pulse due to SS-WTT mapping, thus a temporal waveform with its shape identical to the shaped optical spectrum is generated. Finally, the temporal waveform is sampled by an oscilloscope and the data are sent to the DSP, where the SPR envelope is extracted at high speed and high resolution.

III. EXPERIMENTAL RESULTS

The experimental setup of the RI sensing system based on a TFBG is shown in Fig. 3. A frequency-domain mode-locking (FDML) laser (as shown in the dashed box) is used to provide a frequency swept optical pulse train with a high repetition frequency and large wavelength scanning bandwidth. The mode locking is realized by a sinusoidal signal from a signal generator (SG). A polarization controller (PC1) at the output of the FDML laser source is used to adjust the polarization state of the output pulses into a P-polarization state, so that the SPR-effect can be effectively excited in the sensing element. In our proposed RI

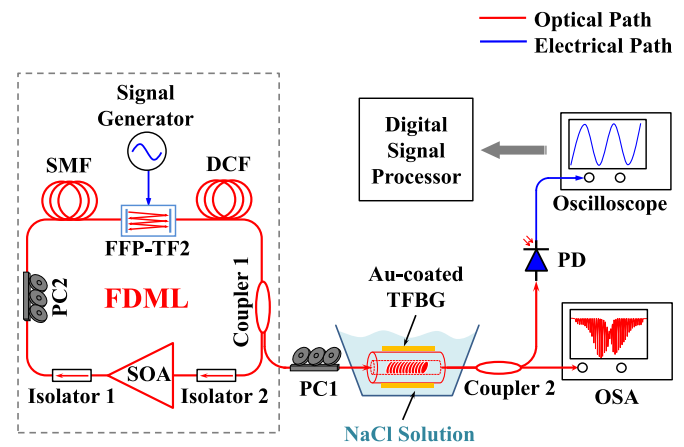


Fig. 3. Experimental setup. The dashed box shows the structure of an FDML laser.

sensing system, the sensing element is an Au-coated TFBG. The TFBG is fabricated in a commercial single-mode-fiber (SMF) with a length of about 30 mm and a tilted angle of 18 degree. To excite the SPR, an Au-coating with a thickness of 50 nm is planted on the surface of the TFBG. It should be noted that we use a tilted angle of 18 degree is to make the wavelength of the dip approximately locate at about 1550 nm when the ambient RI is 1.3325 which is close to the central wavelength of the light wave from the FDML laser source. The spectrum of the frequency-swept optical pulse generated by the FDML laser source is shaped by the Au-coated TFBG-SPR with the RI information encoded in the spectrum. The spectrally shaped optical signal is split into two paths by a 20:80 optical coupler with the 20% path being sent into an OSA to monitor the optical spectrum changes and the 80% path launched into a PD, at which a temporal waveform with its shape identical to the shaped spectrum is generated. A real-time oscilloscope which is synchronized by the SG is employed to sample the temporal waveform, which is processed in a DSP to extract the envelope where the dip is located. Due to the high resolution and high speed of the real-time oscilloscope and the DSP, the RI resolution and the sensing speed of the proposed sensing system is greatly enhanced compared with a conventional interrogation approach using an OSA.

In the FDML laser source, as shown in the dashed box, a semiconductor optical amplifier (SOA) provides a broadband optical gain, and two isolators at the output and the input of the SOA are used to ensure the light has a single operation direction in the laser cavity. A polarization controller (PC2) at the output of the isolator1 is used to adjust the polarization state of the light so that an effective amplification can be achieved. The length of the single-mode-fiber (SMF) used in the light source system is about 7.95 km long and an 877 m long dispersion compensating fiber (DCF) is utilized to compensate for the dispersion to make the laser cavity dispersion free. The key component in the FDML laser system is the wavelength selecting component, a fiber Fabry-Perot tunable filter (FFP-TF2), which is driven by a sinusoidal signal generated by the SG. The optical

signal at the output of FFP-TF2 is separated by a 40:60 optical coupler, with the 40% portion used as the FDML laser output and the 60% portion fed back to the laser cavity for a further amplification.

In order to achieve Fourier domain mode locking, the FFP-TF2 inside the laser cavity must be driven at a frequency that is equivalent to N times of the fundamental cavity frequency, which is given by

$$f_{drive} = N \cdot f_{cav} = N \cdot \frac{c}{n_{core} \cdot (L_{SMF} + L_{DCF})} \quad (1)$$

where N is an integer, c is the light speed in vacuum, n_{core} is the RI of the fiber core (here we assume that the fiber core RI difference between the SMF and DCF is small and negligible), L_{SMF} and L_{DCF} are the physical lengths of the SMF and DCF, respectively.

In our experiment, a sinusoidal function used as a drive signal is applied to FFP-TF2 and the instantaneous output wavelength can be expressed by

$$\lambda_c(t) = A [V_{pp} \cdot \sin(2\pi f_{drive}t) + V_{DC}] + \lambda_0 \quad (2)$$

where A is the tuning sensitivity of FFP-TF2, V_{pp} is the peak-to-peak voltage of the drive signal which decides the wavelength scanning bandwidth of the laser source, f_{drive} is the drive frequency of the sinusoidal signal, V_{DC} is the direct current that decides the central wavelength of the laser source, and λ_0 is the initial wavelength without applying the drive signal and V_{DC} . The values of V_{DC} and the V_{pp} applied to FFP-TF2 in our experiment are 4.98 V and 7 V, respectively. Therefore, the central wavelength of the output optical pulse generated by the FDML laser source will be located at 1550 nm and a wavelength scanning bandwidth of 63 nm of the output optical pulse is achieved. According to (1), the combination of the 7.95 km long SMF and 877 m long DCF will lead to a fundamental cavity frequency equals to 23.496 kHz (here we choose the integer N to be 1), so that the output optical pulse generated by the FDML laser will have a repetition frequency of 23.496 kHz. On the other hand, due to the use of a high speed frequency swept laser, the proposed RI sensing system will have a high sensing speed, which equals to the repetition frequency of the frequency swept laser source.

A pulse train from the FDML laser source with a repetition frequency of 23.496 kHz is applied to the TFBG-SPR. The blue curve in Fig. 4 shows the output spectrum of the light from the FDML laser source. We can see that the output optical pulse generated by the FDML laser source has a 63 nm scanning bandwidth and there are two sharp peaks at 1520 and 1583 nm. The cause of these two sharp peaks is due to the adoption of the sinusoidal drive function, as given in (2), to drive FFP-TF2 inside the FDML laser source. For an identical time interval, the instantaneous output wavelength of the FDML laser source will be located at 1520 and 1583 nm (corresponding to the maximum voltage and the minimum voltage of the sinusoidal drive function) for a longer time. Meanwhile, due to the principle of the integral of power over time of the charge-coupled device (CCD) inside the OSA, a longer integration time means a larger optical power and as a result, the output spectrum of the FDML

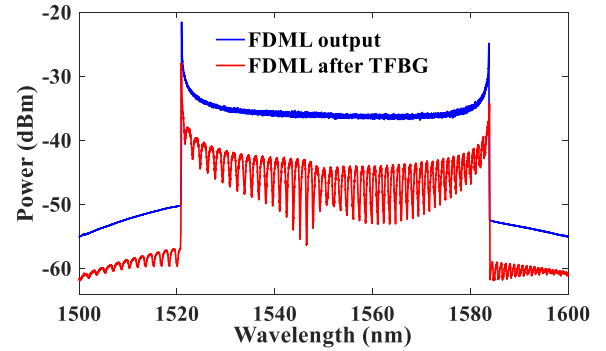


Fig. 4. Blue: The output optical spectrum from the FDML laser source. Red: The optical spectrum after being spectrally shaped by the TFBG-SPR.

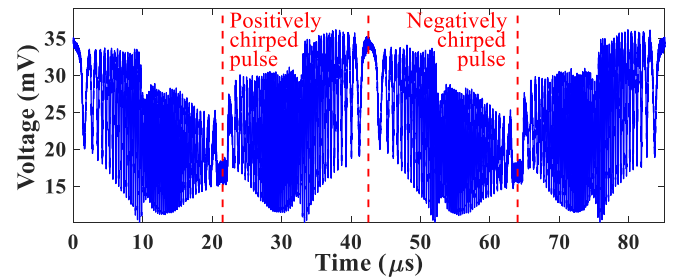


Fig. 5. Microwave waveform within two cycles obtained at the output of the PD.

laser source will have two sharp peaks at the two sides of the scanning bandwidth.

The red curve in Fig. 4 shows the output spectrum from the TFBG-SPR. By spectral shaping, the output spectrum from the FDML laser source is shaped by the TFBG-SPR with the RI information encoded in the spectrum. The spectrally shaped optical signal is launched into a PD, at which a temporal waveform with its shape identical to the shaped spectrum is generated. Fig. 5 shows the microwave waveform sampled by the real-time oscilloscope within two cycles. We can see that the microwave waveform includes two symmetrical pulses in one cycle since a sinusoidal signal is used to drive FFP-TF2 inside the FDML laser source. When the instantaneous voltage of the sinusoidal signal increases from the minimum value to the maximum value, the instantaneous wavelength of the tunable filter inside the FDML laser source will shift from 1583 nm to 1520 nm, a positively chirped optical pulse is generated. When the instantaneous voltage decreases from the maximum value to the minimum value, the instantaneous wavelength of the tunable filter will shift from 1520 nm to 1583 nm, a negatively chirped optical pulse is generated. The spectrum of the optical pulse from the FDML laser source is shaped by the TFBG-SPR and a dip induced by the SPR effect is produced. By wavelength to time mapping, the shaped spectrum is converted to an electrical waveform where a dip is located in its envelope.

In processing the signal at the output of the TFBG-SPR, we consider the spectrum of the signal is amplitude modulated with a dip in the envelope. After SS-WTT mapping, the spectrum is converted to a temporal signal with the cladding modes of

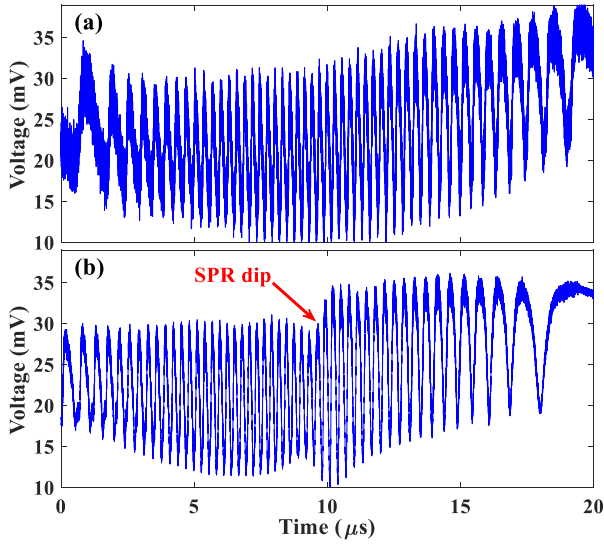


Fig. 6. (a) A positively chirped pulse after spectrally shaped by a TFBG without SPR. (b) A positively chirped pulse after spectrally shaped by a TFBG with SPR.

the TFBG-SPR as a high frequency signal while the envelope as a low frequency signal that amplitude modulates the high frequency signal. In order to extract the SPR envelope, the DSP is used to filter out the high frequency component to get the low frequency component. After being processed by the DSP, the SPR envelope is extracted.

Fig. 6(a) shows a positively chirped pulse after spectrally shaped by a TFBG without SPR. Due to the use of a sinusoidal function to drive the FDML laser source, the instantaneous output wavelength from the FDML laser source and time will establish a nonlinear relationship which will lead to a relatively low frequency component at two sides of the microwave waveform (corresponding to the maximum and the minimum voltage of the sinusoidal function). The positively chirped pulse in Fig. 6(a) can be described as

$$T_{TFBG}(t) = B + \cos \left[2\pi \frac{C \sin(2\pi f_{drive} t)}{D} \right] \quad (3)$$

where B is the DC component of the microwave signal, C is half of the scanning bandwidth, f_{drive} is the drive frequency of the FDML laser source, and D is the wavelength interval of the cladding modes of the TFBG.

In order to realize the extraction of the SPR envelope, the sampled microwave waveform from the real-time oscilloscope (as shown in Fig. 5) is sent to the DSP where the electrical spectrum of the sampled microwave waveform is analyzed. We select one of the positively chirped pulses to analyze its electrical spectrum. The selected waveform is shown in Fig. 6(b), a dip can be found in the SPR envelope and the waveform is given by

$$T_{TFBG-SPR}(t) = SPR(t) \cdot \left\{ B + \cos \left[2\pi \frac{C \sin(2\pi f_{drive} t)}{D} \right] \right\} \quad (4)$$

where $SPR(t)$ is the SPR envelope. To highlight the dip information, a Gaussian window is applied to the temporal waveform.

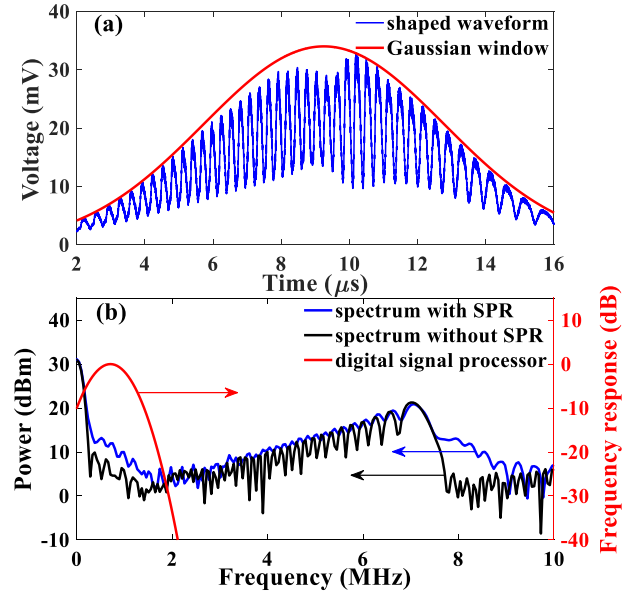


Fig. 7. (a) Blue: The positively chirped optical pulse after shaped by a Gaussian window; Red: The Gaussian window used to shape the microwave waveform. (b) Blue and black curves are the electrical spectrum of the Gaussian window shaped waveform with and without SPR; Red curve is the frequency response of the digital filter.

The Gaussian window and the shaped waveform are shown in Fig. 7(a). Mathematically, the shaped waveform is expressed as

$$T'_{TFBG-SPR}(t) = \exp \left[-\frac{(t-t_0)^2}{2E^2} \right] \cdot SPR(t) \cdot \left\{ B + \cos \left[2\pi \frac{C \sin(2\pi f_{drive} t)}{D} \right] \right\} \quad (5)$$

where t_0 and E are the central time position and the time width of the Gaussian window. Fast Fourier transform (FFT) is performed to the shaped waveform and an electrical spectrum is acquired. The blue and black curves in Fig. 7(b) are the electrical spectra of the microwave waveforms with and without a dip after shaped by a Gaussian window, respectively. After shaped by a Gaussian window, the amplitude of the low frequency component of the waveform without a dip is significantly compressed compared to that with a dip, while the high frequency component of these two waveforms are approximately equivalent. The shaped microwave waveform is then processed in the DSP where a digital low-pass filter with a Gaussian function is implemented. The red curve in Fig. 7(b) shows the frequency response of the Gaussian filter. By adjusting the central frequency and the bandwidth of the Gaussian filter, the high frequency component is filtered out. Here, the central frequency and the 3-dB bandwidth of the Gaussian filter are selected to be 0.705 MHz and 0.7 MHz, respectively.

After filtering out the high frequency component, the filtered microwave waveform is recovered through performing an inverse fast Fourier transform (IFFT) to the filtered electrical

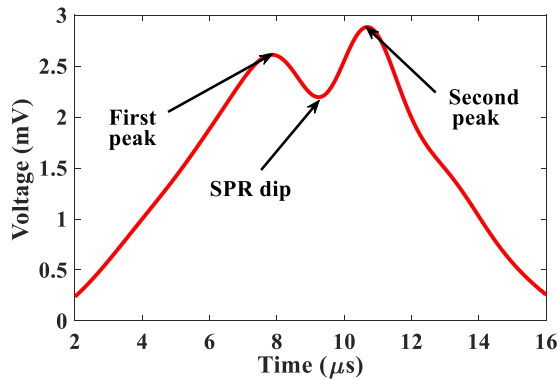


Fig. 8. The recovered microwave waveform.

spectrum. The recovered signal is expressed as

$$T_{TFBG-SPR}''(t) = B \cdot \exp\left[-\frac{(t-t_0)^2}{2E^2}\right] \cdot SPR(t) \quad (6)$$

and the recovered waveform is shown in Fig. 8. From the recovered waveform we can see that the high frequency component of the initial microwave waveform that corresponds to the cladding modes of the TFBG-SPR spectrum is removed and the extraction of the SPR envelope is achieved. Two peaks (we call them the first peak and the second peak here) and a dip in the envelope can be clearly seen. The filtered waveform agrees well with the envelope of the Gaussian window shaped waveform shown in Fig 7(a).

To evaluate the sensing performance of the proposed RI sensor, we immerse the Au-coated TFBG into a NaCl solution with different concentrations. Through increasing the concentration of the NaCl solution, the RI value of the NaCl solution is increased correspondingly. Fig. 9(a) shows the recovered signals when the RI value of the NaCl solution is increased from 1.3326 to 1.3593. As the ambient RI changes, the two peaks and the dip in the envelope are shifted towards a smaller time location.

By measuring the shift of the dip in the SPR envelope, the sensing information is demodulated. Fig. 9(b) shows the RI sensing curves. As can be seen when the Au-coated TFBG is immersed in a NaCl solution with different concentrations corresponding to different ambient RI values, different time shifts (normalized) are obtained. In our experiment, the time shifts of the two peaks and the dip on the envelope are estimated, respectively. The symbols with red, blue and black color are the experimentally measured time shifts of the first peak, the dip and the second peak from the extracted envelope, respectively, meanwhile, when different regions of the envelope are under measured, different RI sensitivity and RI resolution can be achieved. As can be seen from Fig. 9(b), the first peak on the extracted envelope is shifted from $3.762 \mu\text{s}$ to $0 \mu\text{s}$, the dip is shifted from $3.823 \mu\text{s}$ to $0 \mu\text{s}$ and the second peak is shifted from $3.227 \mu\text{s}$ to $0 \mu\text{s}$. The RI sensitivity of the first peak, the dip and the second peak are calculated to be $140.465 \mu\text{s}/\text{RIU}$, $142.496 \mu\text{s}/\text{RIU}$ and $122.859 \mu\text{s}/\text{RIU}$, respectively. At the same time, considering the sampling rate of the real-time

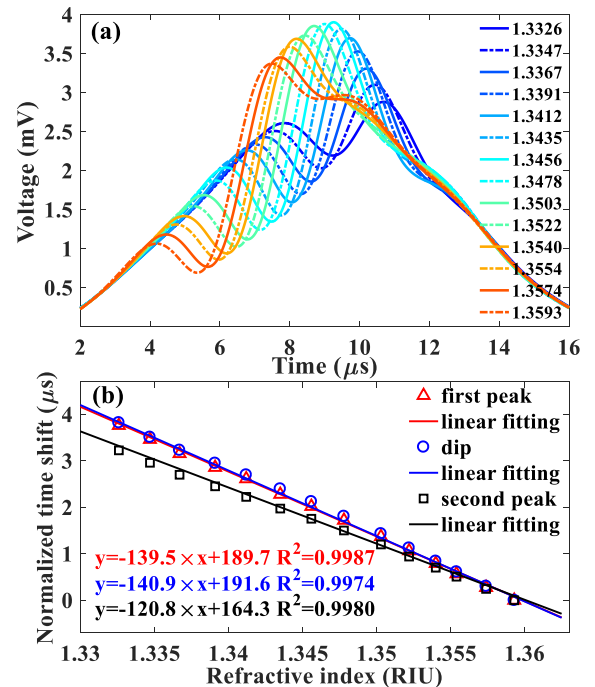


Fig. 9. (a) The extracted envelopes versus the ambient RI change; (b) time shifts of the first peak, the dip and the second peak on the envelope versus ambient RI change. The symbols with three different colors are the experimental results and the curves with three different colors are the results of the linear fitting.

oscilloscope is 6.25 GS/s , the RI resolution of the first peak, the dip and the second peak are calculated to be $1.139 \times 10^{-6} \text{ RIU}$, $1.123 \times 10^{-6} \text{ RIU}$ and $1.302 \times 10^{-6} \text{ RIU}$, respectively. Using a high speed frequency swept laser with a repetition frequency of 23.496 kHz , the sensing speed of the proposed sensing system is as high as 23.496 kHz . To achieve a better demodulating performance, the RI sensitivity can be further improved by reducing the repetition frequency of the FDM laser source or using a dispersion element with a large dispersion coefficient to broaden the output optical pulses generated by the frequency swept laser. On the other hand, the RI resolution can be improved by using a PD with a larger response bandwidth and taking the advantage of the sampling rate of the real-time oscilloscope.

IV. CONCLUSION

We have proposed and experimentally demonstrated a new approach to demodulate the RI information based on a TFBG-SPR by using a microwave photonics technique at a high-speed and high-resolution. Instead of measuring the wavelength shift or the intensity change in the optical domain by using an OSA with low accuracy and resolution, we converted the spectrum of the TFBG-SPR to the time domain based on SS-WTT mapping. A real-time oscilloscope was used to sample the microwave waveform in the time domain and a DSP was used to extract the SPR envelope. Through monitoring the time shift of the extracted SPR envelope, the continuous demodulation of the sensing information was achieved. The proposed RI sensing

system was experimentally demonstrated. Three different regions of the extracted envelope were measured to estimate the RI resolution and the RI sensitivity. The optimal RI resolution and sensitivity of 1.123×10^{-6} RIU and $142.496 \mu\text{s}/\text{RIU}$ at a high speed of 23.496 kHz were achieved by measuring the time shifts of the dip from the extracted envelope.

REFERENCES

- [1] T. Guo, C. Chen, and J. Albert, "Non-uniform-tilt-modulated fiber Bragg grating for temperature-immune micro-displacement measurement," *Meas. Sci. Technol.*, vol. 20, no. 3, Feb. 2009, Art. no. 034007.
- [2] T. Guo, L. Shao, H. Y. Tam, P. A. Albert, and J. Albert, "Tilted fiber grating accelerometer incorporating an abrupt biconical taper for cladding to core recoupling," *Opt. Exp.*, vol. 17, no. 23, pp. 20651–20660, Nov. 2009.
- [3] M. Li, L. Shao, J. Albert, and J. Yao, "Tilted fiber Bragg grating for chirped microwave waveform generation," *IEEE Photon. Technol. Lett.*, vol. 23, no. 5, pp. 314–316, Mar. 2011.
- [4] D. W. Kim, Y. Zhang, K. L. Cooper, and A. Wang, "Fibre-optic interferometric immuno-sensor using long period grating," *Electron. Lett.*, vol. 42, no. 6, pp. 324–325, Mar. 2006.
- [5] Y. Cao *et al.*, "Resolution-improved in situ DNA hybridization detection based on microwave photonic interrogation," *Opt. Exp.*, vol. 23, no. 21, pp. 27061–27070, Oct. 2015.
- [6] Y. Cao *et al.*, "High-resolution and temperature-compensational HER2 antigen detection based on microwave photonic interrogation," *Sensor Actuators B, Chem.*, vol. 245, pp. 583–589, Jun. 2017.
- [7] J. Homola, "Surface plasmon resonance sensors for detection of chemical and biological species," *Chem. Rev.*, vol. 108, no. 2, pp. 462–493, Jan. 2008.
- [8] M. Piliarik and J. Homola, "Surface plasmon resonance (SPR) sensors: Approaching their limits?" *Opt. Exp.*, vol. 17, no. 19, pp. 16505–16517, Sep. 2009.
- [9] A. Shalabney and I. Abdulhalim, "Sensitivity-enhancement methods for surface plasmon sensors," *Laser Photon. Rev.*, vol. 5, no. 4, pp. 571–606, Jul. 2011.
- [10] C. Caucheteur, T. Guo, and J. Albert, "Review of plasmonic fiber optic biochemical sensors: Improving the limit of detection," *Analytical Bioanalytical Chem.*, vol. 407, no. 14, pp. 3883–3897, May 2015.
- [11] T. Guo *et al.*, "Highly sensitive detection of urinary protein variations using tilted fiber grating sensors with plasmonic nanocoatings," *Biosensors Bioelectronics*, vol. 78, pp. 221–228, Apr. 2016.
- [12] T. Guo, F. Liu, Y. Liu, N. Chen, B. Guan, and J. Albert, "In-situ detection of density alteration in non-physiological cells with polarimetric tilted fiber grating sensors," *Biosensors Bioelectronics*, vol. 55, pp. 452–458, May 2014.
- [13] T. Guo, F. Liu, B. Guan, and J. Albert, "Tilted fiber grating mechanical and biochemical sensors," *Opt. Laser Technol.*, vol. 78, pp. 19–33, Apr. 2016.
- [14] J. Lao *et al.*, "In situ plasmonic optical fiber detection of the state of charge of supercapacitors for renewable energy storage," *Light Sci. Appl.*, vol. 7, no. 34, p. 34, Jul. 2018.
- [15] N. Aissaoui, L. Bergaoui, J. Landoulsi, J. F. Lambert, and S. Boujday, "Silane layers on silicon surfaces: Mechanism of interaction, stability, and influence on protein adsorption," *Langmuir*, vol. 28, no. 1, pp. 656–665, Nov. 2011.
- [16] W. Si and A. Aksimentiev, "Nanopore sensing of protein folding," *ACS Nano*, vol. 11, no. 7, pp. 7091–7100, Jul. 2017.
- [17] J. Yao, "Microwave photonics," *J. Lightw. Technol.*, vol. 27, no. 3, pp. 314–335, Feb. 2009.
- [18] J. Copmany and D. Novak, "Microwave photonics combines two worlds," *Nature Photon.*, vol. 1, pp. 319–330, Jun. 2007.
- [19] P. Ghelfi *et al.*, "A fully photonics-based coherent radar system," *Nature*, vol. 507, pp. 341–345, Mar. 2014.
- [20] H. Deng, W. Zhang, and J. Yao, "High-speed and high-resolution interrogation of a silicon photonic microdisk sensor based on microwave photonic filtering," *J. Lightw. Technol.*, vol. 36, no. 19, pp. 4243–4249, Oct. 2018.
- [21] H. Deng, P. Lu, S. J. Mihailov, and J. Yao, "High-speed and high-resolution interrogation of a strain and temperature random grating sensor," *J. Lightw. Technol.*, vol. 36, no. 23, pp. 5587–5592, Dec. 2018.
- [22] C. Wang and J. Yao, "Simultaneous optical spectral shaping and wavelength-to-time mapping for photonic microwave arbitrary waveform generation," *IEEE Photon. Technol. Lett.*, vol. 21, no. 12, pp. 793–795, Jun. 2009.
- [23] C. Wang and J. Yao, "Chirped microwave pulse generation based on optical spectral shaping and wavelength-to-time mapping using a Sagnac loop mirror incorporating a chirped fiber Bragg grating," *J. Lightw. Technol.*, vol. 27, no. 16, pp. 3336–3341, Aug. 2019.
- [24] F. Coppinger, A. S. Bhushan, and B. Jalali, "Photonic time stretch and its application to analog-to-digital conversion," *IEEE Trans. Microw. Theory*, vol. 47, no. 7, pp. 1309–1314, Jul. 1999.

Guangying Wang received the B.Eng. degree in optoelectronic information science and engineering from the Guangdong University of Technology, Guangzhou, China, in 2017. He is currently working toward the Ph.D. degree in optical engineering with the Institute of Photonics Technology, Jinan University, Guangzhou, China.

His current research interests include microwave photonics sensing and signal processing.

Yuan Cao received the B.S. degree from the Dalian University of Technology, Dalian, China, in 2011, and the Ph.D. degree from Jinan University, Guangzhou, China, in 2016. He is currently a Lecturer with the Institute of Photonics Technology, Jinan University, Guangzhou, China.

His research interests include microwave photonics signal processing & applications and optical biosensors.

Nan Hu received the B. Eng. degree in optoelectronic information engineering from Nanjing Xiaozhuang University, Nanjing, China, in 2017. She is currently working toward the master's degree with the Institute of Photonics Technology, Jinan University, Guangzhou, China.

Xuejun Zhang received the Ph.D. degree in biomedical physics and biomedical information technology from Jinan University, Guangzhou, China, in 2019. He is currently working with the Center for Advanced Biomedical Imaging and Photonics Department of Medicine, Beth Israel Deaconess Medical Center, Harvard University, as a Research Fellow. His research interests include plasmonics, biophotonics, fiber gratings, and fiber sensors.

Shaochen Duan is currently working toward the undergraduate degree with the Institute of Photonics Technology, Jinan University, Guangzhou, China.

Tuan Guo received the B.Sc. and M.Sc. degrees in electrical engineering from Xi'an Shiyou University, Xi'an, China, in 2001 and 2004, respectively, and the Ph.D. degree in optics from Nankai University, Tianjin, China, in 2007. He is currently a Professor with the Institute of Photonics Technology, Jinan University, Guangzhou, China. Thereafter, he was a Postdoctoral Fellow with the Department of Electronics, Carleton University, Canada and the Photonics Research Centre, The Hong Kong Polytechnic University, Hong Kong. He joined Jinan University as an Associate Professor in 2011 and was promoted to a Full Professor in 2014. He has authored or coauthored more than 100 peer-reviewed journal articles mainly in *Biosensors and Bioelectronics*, *Analytical Chemistry*, *Analytical and Bioanalytical Chemistry*, *Applied Physics Letters*, *Optics Letters*, *Optics Express*, and IEEE series. He holds 15 patents and many other pending patents. His research activities include optical fiber sensors, fiber lasers, fiber gratings, plasmonics, biophotonics, microfluidic, and microcavity devices. He was an Associated Editor for the *Journal of Sensors* from 2010 to 2014 and a Guest Editor for a Special Issue on "Recent Advances in Fiber Bragg Grating Sensing" on MDPI Sensors in 2016. He is a Member of the Optical Society of America (OSA).

Xinhuan Feng received the B.Sc. degree from Physics Department, Nankai University, Tianjin, China, in 1995, and the M.Sc. and Ph.D. degrees from the Institute of Modern Optics, Nankai University, in 1998 and 2005, respectively.

From 2005 to 2008, she was a Postdoctoral Fellow with Photonics Research Centre, The Hong Kong Polytechnic University, Hong Kong. Since March 2009, she has been a Professor with the Institute of Photonics Technology, Jinan University, Guangzhou, China. Her research interests include various fiber active and passive devices and their applications, and microwave photonic signal processing.

Bai-Ou Guan received the B.Sc. degree in applied physics from Sichuan University, Chengdu, China, in 1994, and the M.Sc. and Ph.D. degrees in optics from Nankai University, Tianjin, China, in 1997 and 2000, respectively. From 2000 to 2005, he was with the Department of Electrical Engineering, The Hong Kong Polytechnic University, Hong Kong, first as a Research Associate, then as a Postdoctoral Research Fellow. From 2005 to 2009, he was with the School of Physics and Optoelectronic Engineering, Dalian University of Technology, Dalian, as a Full Professor. In 2009, he joined Jinan University, Guangzhou, China, where he founded the Institute of Photonics Technology. His current research interests include fiber optic devices and technologies, optical fiber sensors, biomedical photonic sensing and imaging, and microwave photonics. He has authored or coauthored more than 230 technical papers in peer-reviewed international journals and presented more than 30 invited talks at major international conferences. He received the Distinguished Young Scientist Grant from Natural Science Foundation of China (NSFC) in 2012. He is a Member of OSA, and has served as the General Chair/Co-Chair, Technical Program Committee or Subcommittee Chair/Co-Chair for more than 10 international conferences.

Jianping Yao (M'99–SM'01–F'12) received the Ph.D. degree in electrical engineering from the Université de Toulon et du Var, Toulon, France, in December 1997. He is a Distinguished University Professor and University Research Chair with the School of Electrical Engineering and Computer Science, University of Ottawa, Ottawa, ON, Canada. From 1998 to 2001, he was with the School of Electrical and Electronic Engineering, Nanyang Technological University, Singapore, as an Assistant Professor. In December 2001, he joined the School of Electrical Engineering and Computer Science, University of Ottawa as an Assistant Professor, where he was promoted to an Associate Professor in May 2003, and a Full Professor in May 2006. He was appointed the University Research Chair in Microwave Photonics in 2007. In June 2016, he was conferred the title of Distinguished University Professor of the University of Ottawa. From July 2007 to June 2010 and from July 2013 to June 2016, he was the Director of the Ottawa–Carleton Institute for Electrical and Computer Engineering. He has authored or coauthored more than 620 research papers including more than 360 papers in peer-reviewed journals and more than 260 papers in conference proceedings.

Dr. Yao is the Editor-in-Chief for the IEEE PHOTONICS TECHNOLOGY LETTERS, a Topical Editor for *Optics Letters*, an Associate Editor for *Science Bulletin*, a Steering Committee Member for the IEEE JOURNAL OF LIGHTWAVE TECHNOLOGY, and an Advisory Editorial Board Member for *Optics Communications*. He was a Guest Editor of a Focus Issue on Microwave Photonics in *Optics Express* in 2013, a Lead-Editor of a Feature Issue on Microwave Photonics in *Photonics Research* in 2014, and a Guest Editor of a Special Issue on Microwave Photonics in the IEEE JOURNAL OF LIGHTWAVE TECHNOLOGY in 2018. He is currently the Chair of the IEEE Photonics Ottawa Chapter and is the Technical Committee Chair of IEEE MTT-3 Microwave Photonics. He was a Member of the European Research Council Consolidator Grant Panel in 2016, the Qualitative Evaluation Panel in 2017, and a Member of the National Science Foundation Career Awards Panel in 2016. He was also a chair of a number of international conferences, symposia, and workshops, including the Vice Technical Program Committee (TPC) Chair of the 2007 IEEE Topical Meeting on Microwave Photonics, TPC Co-Chair of the 2009 and 2010 Asia-Pacific Microwave Photonics Conference, TPC Chair of the High-Speed and Broadband Wireless Technologies Subcommittee of the IEEE Radio Wireless Symposium 2009–2012, TPC Chair of the Microwave Photonics Subcommittee of the IEEE Photonics Society Annual Meeting 2009, TPC Chair of the 2010 IEEE Topical Meeting on Microwave Photonics, General Co-Chair of the 2011 IEEE Topical Meeting on Microwave Photonics, TPC Co-Chair of the 2014 IEEE Topical Meetings on Microwave Photonics, and General Co-Chair of the 2015 and 2017 IEEE Topical Meeting on Microwave Photonics. He was also a Committee Member for a number of international conferences, such as IPC, OFC, BGPP, and MWP. He was the recipient of the 2005 International Creative Research Award of the University of Ottawa, the 2007 George S. Glinski Award for Excellence in Research, a Natural Sciences and Engineering Research Council of Canada Discovery Accelerator Supplements Award in 2008, an inaugural OSA Outstanding Reviewer Award in 2012, and the Award for Excellence in Research 2017–2018 of the University of Ottawa. He was one of the top ten reviewers of IEEE/OSA JOURNAL OF LIGHTWAVE TECHNOLOGY (2015–2016). He was an IEEE MTT-S Distinguished Microwave Lecturer for 2013–2015. He is a registered Professional Engineer of Ontario. He is a Fellow of the Optical Society of America, the Canadian Academy of Engineering, and the Royal Society of Canada.